JOURNAL OF MATERIALS SCIENCE **39** (2004) 5747–5754

Structural characterisation of apatite coatings

K. D. ROGERS*, S. E. ETOK
Department of Materials & Medical Sciences, Cranfield University, Shrivenham, Swindon, Wiltshire SN6 8LA, UK
E-mail: k.d.rogers@rmcs.cranfield.ac.uk

R. SCOTT
Biomet-Merck Ltd., Dorcan, Swindon, Wiltshire SN3 5HY, UK

The current, most frequently employed, commercial route to produce hydroxyapatite prosthetic coatings is plasma spraying. However, this has several important limitations especially for textured surfaces. Low temperature methods of coating fabrication such as cathodic electrodeposition are attractive alternatives. However, quantitative characterisation of the phase composition of thin electrodeposited coatings can be problematic. An X-ray diffraction method, which provides quantitative compositional information without reference to external or internal standards, is introduced and validated. The method can also be applied when Bragg peaks from the supporting substrate are apparent within the data and preferred orientation can be tolerated. This method has been used to examine in detail the microstructure of electrodeposited coatings which are compared directly with those formed by a commercial plasma spraying process.

We show that, unlike the plasma sprayed coatings, the electrodeposited material consists of a single crystalline phase (hydroxyapatite) and a significantly reduced amorphous phase. The electrodeposited coatings also possess significantly more microstrain and a smaller crystallite size than the corresponding plasma sprayed material.

1. Introduction

In recent years, coating metal orthopaedic implants with bioactive layers to promote fixation has become increasingly common [1]. Fabrication routes that provide control over features such as biocompatibility and bioreactivity through management of coating chemistry and structure are still being developed. Calcium hydroxyapatite (HAP) is thought to be a particularly attractive coating material as it has been shown to induce physiochemical bonding at HAP-bone interfaces and promote bone growth with high growing in rates [2]. The ultimate behavior of the implant i.e., clinical outcome, has been shown to be affected by features such as coating thickness, surface texture, phase purity, bond/mechanical strength, and dissolution properties, although the optimum properties of a coating have yet to be identified.

Current coating fabrication routes include plasma spraying (PS), rf sputtering, CVD, laser ablation and recently sol-gel, although plasma spraying is used to produce most commercially available bioceramic coatings for orthopaedic and dental implants. Advantages of PS include a short cycle time to coat a component and minimal heating of the substrate. However, it is a line-of-sight method that has several disadvantages, including difficulties in achieving a uniform coating thickness on an uneven surface and an inability to coat the inner surface of porous implants. Delamination of the coating caused by internal stresses and mis-match in modulus between the alloy substrate and the coating can occur with thicker coatings. Further, plasma spraying is a relatively expensive and inefficient process to set up and maintain. Coatings are built up from partially melted powder particles, and are thus a heterogeneous mixture of unmelted crystallites of the original stock powder, other crystalline phases (e.g., CaO) and amorphous material [3]. The amorphous material and other phases are significantly more soluble than the hydroxyapatite, and hence these are preferentially dissolved *in vivo*. This can lead to fragmentation of the coating, releasing particles into the surrounding tissues. Porosity can accelerate this process. These particles can potentially contribute to cell-mediated osteolysis. There have also been reports [4] of HAP particles becoming embedded within bearing surfaces of polyethylene acetabular cups, scratching the femoral heads and leading to accelerated wear. Alternatives to plasma spraying are therefore worth investigating.

There is no doubt that producing an adherent, HAP coating using a low temperature process with control over the film microstructure is an attractive goal. Although biomimetic methods have shown some initial

*Author to whom all correspondence should be addressed.

promise [5], a more immediate, commercially scaleable process is required. Electrodeposition (ED) has the potential to provide dense, macroscopically homogenous coatings, with good internal cohesion and adhesion to the implant surface. Particular advantages of electrodeposition for production of bioprosthetic coatings are relatively low costs and energy, low temperatures, ability to coat textured surfaces, and control of thickness & microporosity. It may also enable incorporation of biomolecules forming a sustained release, drug delivery system e.g., it has been shown [6] that lysine attachment may be controlled through the number of OH polar groups (H bonding with protein molecules).

Successful electrodeposition of HAP has been demonstrated previously by groups in China [7], Canada [8] and recently in the U.K. [9]. Initial attempts usually involved the electrodeposition of a non-HAP phase (e.g., brushite, $CaHPO_4 \cdot 2H_2O$) which was subsequently converted to HAP with alkaline solutions or calcinating at $\sim$400°C. Indeed there may be advantages to such a '2 stage' approach for control of film properties such as crystallite morphology through this second step, and thus, work continues in this field [10, 11]. Single stage electrodeposition of HAP was first reported by Shirkhanzadeh [12] and a recent similar process has been developed here. The ED mechanism of HAP deposition is complex and involves combined electrochemical, acid–base and precipitation reactions. Some control of the crystallographic phase formed is afforded by the cathodic current density and interfacial pH which has been previously investigated [13]. The structural characterisation of coatings formed in this manner is critical to optimization of performance.

This work concerns a direct, structural comparison of coatings produced by PS and ED methods examined, in detail, principally by X-ray diffraction. It also introduces a new methodology for reliably determining the quantitative phase composition of coatings *in situ* and thus the crystalline/amorphous ratio ("crystallinity"). This has been shown to be particularily influential in coating fixation and resorption [14].

2. Method

2.1. Coating fabrication

The coatings examined were supported upon titanium test coupons ($\sim$1 cm $\times$ 3 cm $\times$ 0.5 cm) for the ED, and Ti disks (diameter $\sim$2 cm) for the PS. Before coating, each substrate was cleaned in ethanol within an ultrasonic bath, rinsed off with deionized water, and dried by means of a stream of air.

The PS coatings were formed by conventional PS methods. In brief, this consisted of spaying a stock (>98% hydroxyapatite) powder in air with a Plasma-Technic Type F4-MB plasma gun. This used argon as the primary gas, and nitrogen as the secondary gas. The resultant coatings were typically 50–80 μm thick. Characteristics complied with BS ISO 13779-2:2000 ("*Impants for surgery.Hydroxyapatite. Coatings of hydroxyapatite*").

The ED coatings were formed by cathodic electrodeposition within a purpose built chemical bath. The electrolyte liquid (Ca/P ratio of 1.67) was prepared from $CaCl_2 \cdot 2H_2O$ and $NH_4H_2PO_4$ dissolved in deionised water. The temperature of the electrolyte was controlled by means of a thermostat and fixed to 37°C. The pH was adjusted to 6.45 using an NH_4OH solution. The Ti substrate was polarised as the cathode and platinum gauze electrodes employed as the anode.

Coating consisted of repeated cycles of cathodic polarisation and drying. The resultant coatings were typically 3 μm thick. Further details are provided within the Bonemaster® Patent, EP1264606.

2.2. Diffraction analysis

The samples were all analysed with the coatings *in situ* by conventional powder X-ray diffractometry. Diffraction data was collected using a Philips PW1830 diffractometer fitted with a diffracted beam monochromator to produce diffractograms from Cu K_α wavelengths.

Phase identification was performed with reference to the database supplied by the International Centre for Diffraction Data using the software, 'CSM' (Oxford Cryosystems).

Typically, quantitative phase analysis (including amorphous content) has been undertaken with X-ray diffraction but traditionally the methodology has required 'spiking' the sample with a known amount of a highly crystalline phase [15]. This is clearly not appropriate for coatings measured *in situ*. Further, previous methods have usually depended upon measurement of Bragg intensities and assume no preferred orientation and fixed stoichiometry of the HAP relative to the material used as a calibrant [16–18]. We have undertaken quantitative analysis using a whole pattern fitting ('Rietveld') approach [19]. Recently, analyses from studies of glass-ceramic crystallisation processes have indicated how 'standardless' Rietveld analysis can be performed that includes a non-crystalline phase. The theoretical justification for this has been described elsewhere [20] and some examination of PS coatings investigated [21]. We have adopted a similar approach here and also validated the method with reference to known mixtures of crystalline and amorphous CaP phases. Rietveld analysis was undertaken using TOPAS (Bruker–XAS) and the atomic structural models acquired from the Inorganic Crystal Structural Database [22]. In these analyses, the amorphous component was described using an atomic model fixed to that of stoichiometric HAP but with a crystallite size similar in magnitude to that of the lattice parameters. This produced a diffraction pattern with the appearance of that from an amorphous material, i.e., significantly broadened and overlapped diffraction maxima. To provide appropriate and precise values of lattice parameter and apparent crystallite size, these parameter values were refined against diffraction data from an amorphous CaP phase. This is in contrast to previous similar work where only a poor fit could be obtained as the lattice parameters were fixed [23] to stoichiometric HAP. For all subsequent analyses of mixed phases, all the parameters (except for the scale factor) of the amorphous phase were fixed to these values. This may simplify the

precise shape of scattering from the amorphous component [24], but can provide an approximate value for the density of the non-crystalline phase. An influential parameter in this analysis for accurate quantification is appropriate choice of background. The background shape was determined empirically using data from substrates with their coatings removed and this was represented by a 1st order Chebychev polynomial.

The fitting methodology was assessed for accuracy and reliability by repeated, independent determinations of know mixtures of amorphous and crystalline phases. In all refinements, the atomic model parameters (i.e., atomic positions, thermal parameters & occupancies) were fixed throughout. This effectively fixed the absorption coefficients of each phase. Scale factors, lattice parameters, and peak shapes were refined for all crystalline phases. An advantage of this approach is that preferred orientation could also be included and accounted for (in this case using spherical harmonics) in the fitting process. For the ED coatings, the dominant substrate maxima were included as independent analytical peaks without reference to any structural model but were refined simultaneously with the structural phases. Using TOPAS, this effectively excluded the substrate from estimates of coating phase composition.

For microstructural analyses (crystallite size/microstrain), a pseudo-Voigt analytical profile ($K\alpha_1$ & $K\alpha_2$) was fitted to each of the observed diffraction maxima. Fitting quality was assessed using a chi-squared parameter and those of low quality excluded from further analyses, as were adjacent, overlapping peaks. Only the $K\alpha_1$ component was subsequently employed in further analyses. This fitting procedure provided independent estimates of peak position and full width at half maximum (fwhm). Peak broadening attributable to the specimen microstructure was estimated using,

$$\mathrm{fwhm_f} = \left(\mathrm{fwhm_h^2} - \mathrm{fwhm_g^2}\right)^{1/2}$$

where the subscripts f, h & g refer to the structural, observed and instrumental profiles. The instrumental broadening contribution was determined from diffraction data produced from a NIST silicon standard reference material, NBS640b. These structural widths were exploited in a Williamson-Hall analysis [25], which offers assessments of crystallite size and microstrain contributions to the peak widths. The analysis performed here assumed that the microstrain and crystallite domain size was uniform in all crystallographic directions. A similar type of analysis has been performed previously [26] on PS coatings of HAP.

3. Results

In all, we have examined >40 ED coatings and >500 PS coatings by X-ray diffraction. The diffraction data from each group has been consistent. Typical diffraction data is presented in Figs 1 and 2 representing that from PS and ED respectively. The PS data derives from a 60 μm coating (Fig. 1a) and from a significantly thinner coating ($\sim$10 μm) produced using identical processing conditions but interrupted early on in the coating cycle (Fig. 1b). Thus we are able to examine the typical PS surface material (95% penetration depth of CuKα X-rays $\sim$16 μm) and material close to the substrate interface. Fig. 2b presents data from the ED sample that is expanded in Fig. 2a in order to show the HAP peaks more clearly. In both the PS and ED coatings, the dominant crystalline phase of the coating is HAP (although, due to the significantly thinner coating the ED data is dominated by the Ti substrate peaks). Data corresponding to the PS coating shows a clear amorphous phase, the relative magnitude of which is significantly greater for the interrupted coating which also shows a greater amount of extraneous (non-HAP) crystalline phases. These extraneous phases have been identified to include CaO and $Ca_3(PO_4)$. It is also apparent that although the S/N is poorer for the ED coating data there is no evidence of crystalline phases other than HAP.

In order to assess the accuracy of the standardless quantitative analysis, diffraction data from a systematic series of powder samples of known composition were collected and analysed as described above. Fig. 3 shows an example of the data from one such sample and also indicates the components of the fitting process. The fit is of good quality (as indicated by the R_{wp} value – 9.8%) although the data contains small extraneous peaks not accounted for by the models used. Table I contains data for a range of composition standards. In all cases, the ACP values agree within 3%. It should be appreciated that all phases were initially included in all of the analytical refinements. Where a 0 is recorded, the wt% refined to <0.2%.

Reliability was assessed by repeated measurement and analysis of a single sample with a measured composition of 75%HA and 25% ACP. Mean values of HAP wt% content, and lattice parameters of the HAP were found to be 75.8% ($\pm$0.7%) and 9.400 ($\pm$0.001) & 6.899 ($\pm$0.001) respectively as a result of 4 independent analyses. Numbers in parentheses are standard errors and the maximum R_{wp} value was 8.3%.

A summary of the principal structural characteristics of the PS and ED coatings is provided in Table II. This provides data from a randomly selected, full thickness PS coating, the limited thickness PS coating and average values from 40 ED coatings. The HAP/ACP ratio of the PS coatings was observed to show periodic fluctuations with time (period of $\sim$weeks), which corresponded to aging and replacement of the spray nozzle. For the PS material, significantly more ACP is measured near the Ti interface than at the initially exposed surface. The HAP (002) peak width (an indication of crystal size/strain along $\langle 00l \rangle$) is similar for both PS coatings but data from the ED indicates a significantly greater (002) width. The lattice parameters all show small, and mostly insignificant differences between samples with the greatest difference between the upper surface PS and ED coatings.

A pragmatic approach to quantifying preferred orientation has been adopted for simplicity, and a "PO index" derived. This was based upon the ratio of the integrated areas of the (002) and (222) reflections normalised to their random values. Thus if PO = 1, then

TABLE I Comparison of measured compositions with those determined by Rietveld analysis

Weighed amounts				Wt% from XRD analysis			
HAP	ACP	α-$Ca_3(PO_4)_2$	β-$Ca_3(PO_4)_2$	HAP	ACP	α-$Ca_3(PO_4)_2$	β-$Ca_3(PO_4)_2$
100	0	0	0	97.8	2.2	0	0
80	20	0	0	80.5	19.5	0	0
60	40	0	0	59.8	40.2	0	0
40	60	0	0	42.3	57.7	0	0
92.5	0	7.5	0	92.1	0	7.9	0
97.5	0	2.5	0	96.4	0	3.6	0
92.5	0	0	7.5	90.1	0	0	9.9
97.5	0	0	2.5	96.9	0	0	3.1

TABLE II Structural characteristics of typical PS and ED coatings. (PO: preferred orientation index.)

Source	Composition (wt%)	fwhm /° (002)	**a**/nm	σ(**a**)	**c**/nm	σ(**c**)	PO
PS full coating	70%HAP 28%ACP 2% β-$Ca_3(PO_4)_2$	0.156	0.94106	3×10^{-5}	0.68902	3×10^{-5}	0.72
PS partial coating	32%HAP 61% ACP 2% CaO 2% β-$Ca_3(PO_4)_2$ 2% α-$Ca_3(PO_4)_2$	0.156	0.94093	5×10^{-5}	0.68914	4×10^{-5}	0.71
ED	70%HAP 30%ACP	0.247	0.93946	2×10^{-4}	0.68935	2×10^{-4}	2.11

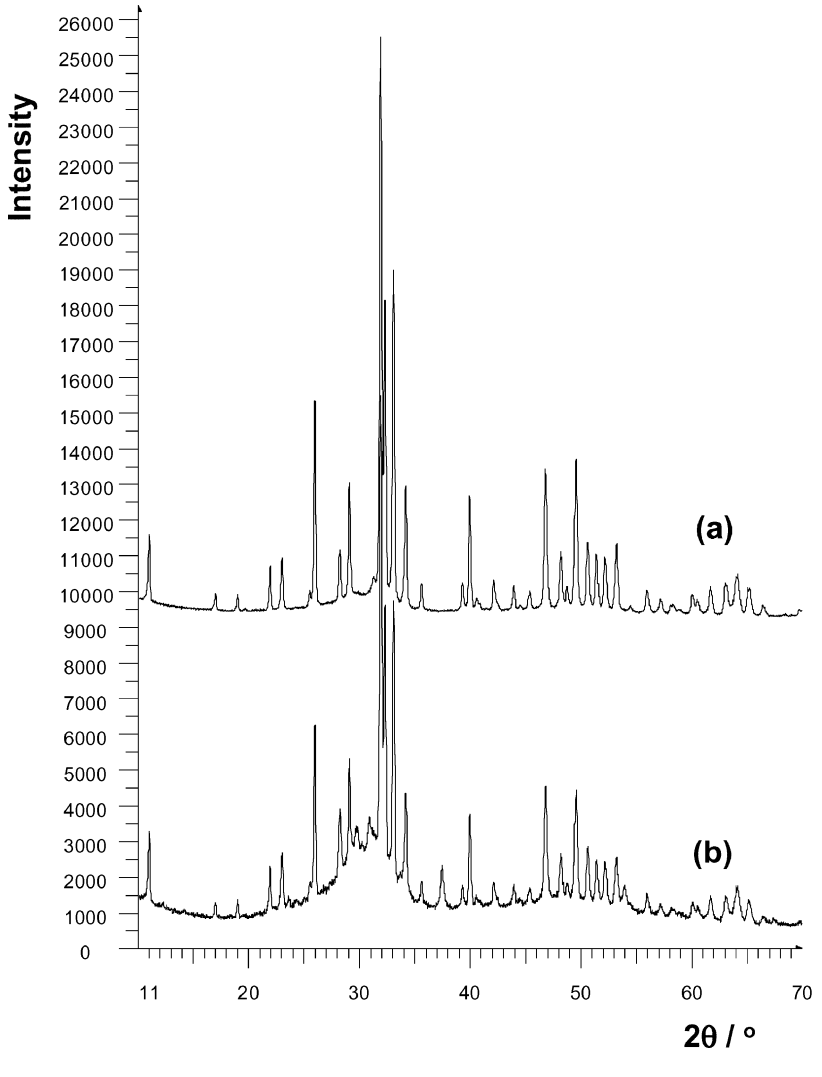

Figure 1 Diffraction data from PS coatings (a) full thickness (~60 μm) and (b) limited thickness (~10 μm).

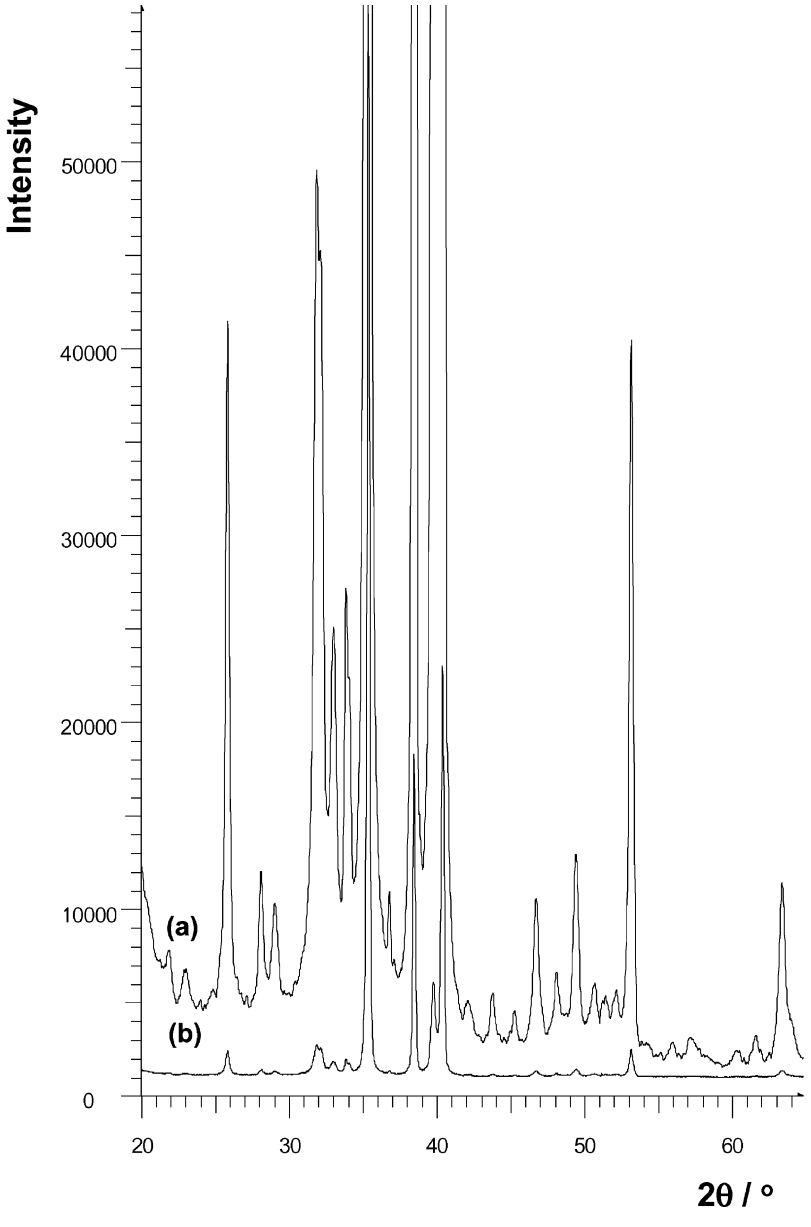

Figure 2 Diffraction data from typical ED coating. Plot (a) is an intensity scaled diffractogram of that presented in (b) to show the HAP diffraction maxima.

this would indicate no preferred orientation. Of note is the increased degree of preferred orientation associated with the ED coatings.

The results of the microstructural characterisations are shown in Fig. 4, which is a Williamson-Hall plot of the peak widths for the PS and ED coatings. Here the magnitude of any microstrain, and crystallite size are indicated by the gradient and intercept of the curves respectively. An intercept of zero suggests that the diffraction data is not broadened by finite crystallite size and this would occur if the crystallites were greater than approximately 0.2 μm.

The limited quality and overlapping substrate peaks of the ED data resulted in significantly fewer peaks from the ED coating being exploited in this analysis. Both PS coatings produced indistinguishable results. Within experimental errors, the data corresponding to the PS coatings indicate that only microstrain effects broaden the peak widths i.e., the crystallite size is in excess of 0.5 μm (the upper limit of size determination). It is difficult to provide definitive, quantitative conclusions regarding the ED coating data due to the limited number of peaks analysed.

4. Discussion and conclusions

These studies have enabled a direct structural comparison of HAP coatings formed by PS and ED techniques. The analytical methodology employed has been shown capable of reliably providing accurate and quantitative compositional information without reference to external or internal standards. It is anticipated that this technique could be applied to a wide range of materials, although mixtures containing phases with very different absorption coefficients may be more challenging. However, in contrast to alternatives, and in the presence of preferred orientation as in the case of ED coatings, this methodology is apparently robust.

The nature of the ED coating material is significantly different to that of the PS. The PS material is

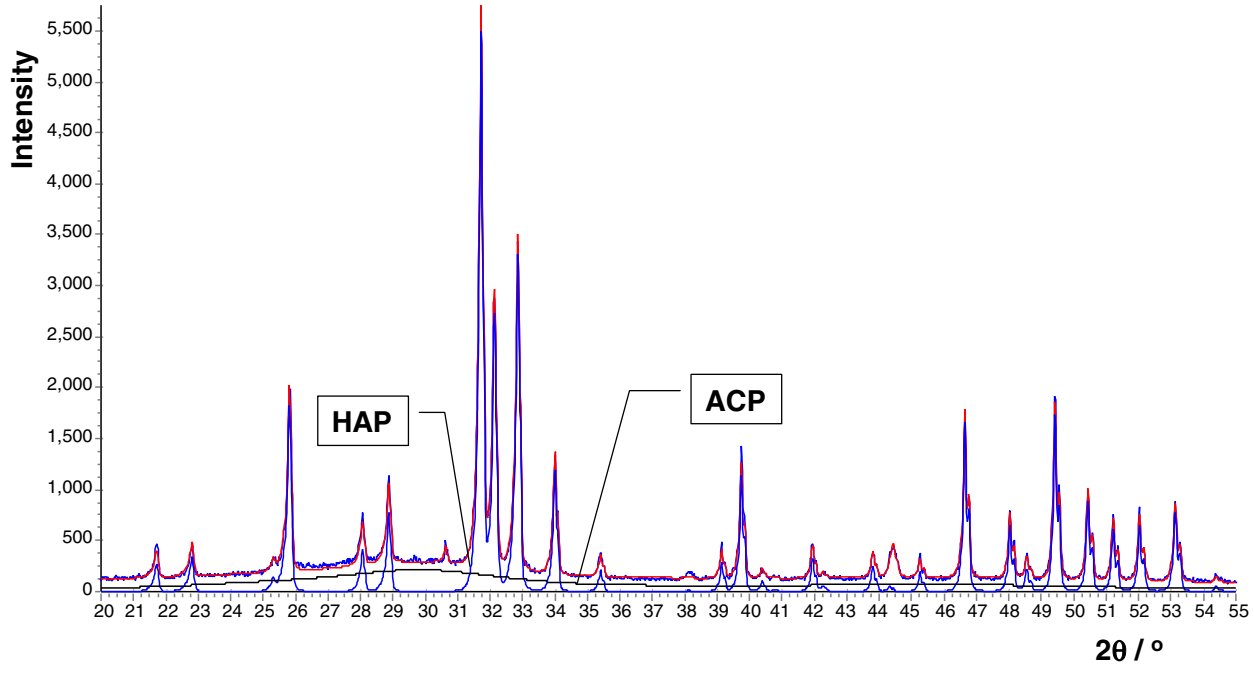

Figure 3 Observed and calculated diffraction data (overlaid) corresponding to known mixture of HAP & ACP (60% HAP). Each component contributing to the calculated data is also shown separately and marked.

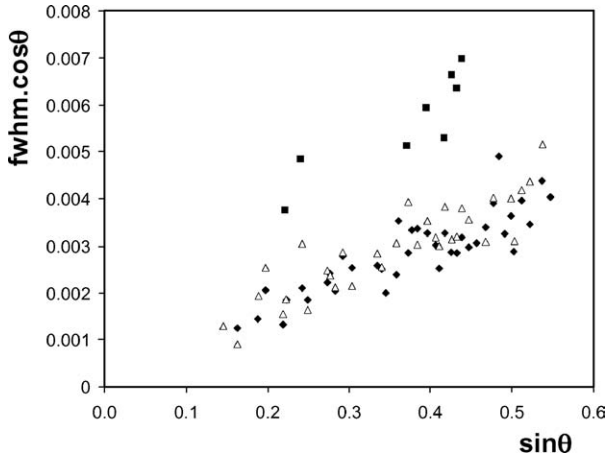

Figure 4 A Williamson-Hall plot representing peak broadening data from (♦) full thickness PS coating, (Δ) limited thickness PS coating and (■) ED coating.

typical of that previously described [26], comprising predominantly of a highly crystalline HAP and ACP mix. Interestingly although the microstrain appears to remain constant through the coating thickness, it is apparent that the amount of ACP and extraneous crystalline phases are significantly greater closer to the Ti interface. We have evidence from an alternative study that any compositional gradient is confined to a region close to the Ti [27]. Such a chemical gradient has been recently observed using micro-Raman methods [28]. However, as there are no significant differences in either lattice parameter for the PS coatings examined, any chemical gradient is most likely associated with phase changes rather than changes to the chemistry of the HAP. This is consistent with the enhanced thermal 'shock' experienced by the particles at the initial stages of coating. A further observation from PS diffraction data was a positive correlation between the (002) d-spacing and (002) peak width. No correlation was found between the HAP/ACP ratio and (002) peak width.

In contrast to the PS material, no extraneous crystalline phases were detected within the ED coatings. In particular, the diffraction data was interrogated for the presence of monetite ($CaHPO_4$) and, in the 2θ region 3–6°, the presence of octacalcium phosphate ($Ca_8H_2(PO_4)_6\ 5H_2O$). This is a similar finding to that of Manso *et al.* [29] who produced ED coatings on thin films of Ti. The crystal quality of the HAP is also poorer than that of the PS with respect to it possessing a smaller crystallite size and greater microstrain. This microstrain is probably the result of mechanical stress associated with direct growth on the substrate and heterogeneous lattice substitutions and vacancies. The ED coating has approximately 3 times the dislocation density as the PS coating and this will undoubtedly result in enhanced dissolution and reactivity of the ED material [30]. However, this will be offset by the reduced dissolution as a result of the smaller amount of ACP in the coating which may also result in a coating with greater integrity.

Previously **a** & **c** have been used to determine the degree of dehydroxyation in PS coatings [21]. However, the lattice parameter differences between the coatings are small, but **a** is significantly smaller for the ED material compared to the PS. This may be due to a particular heteroionic lattice substitution but, because **c** is not significantly different, it is more likely due to a combination of substitutions.

The very much greater degree of preferred orientation of the ED material is expected due to the slower growth process compared to PS. This has been observed previously for direct cathodic formation of HAP [31]. However, the change in degree of texture through the PS coatings observed previously [32] was not

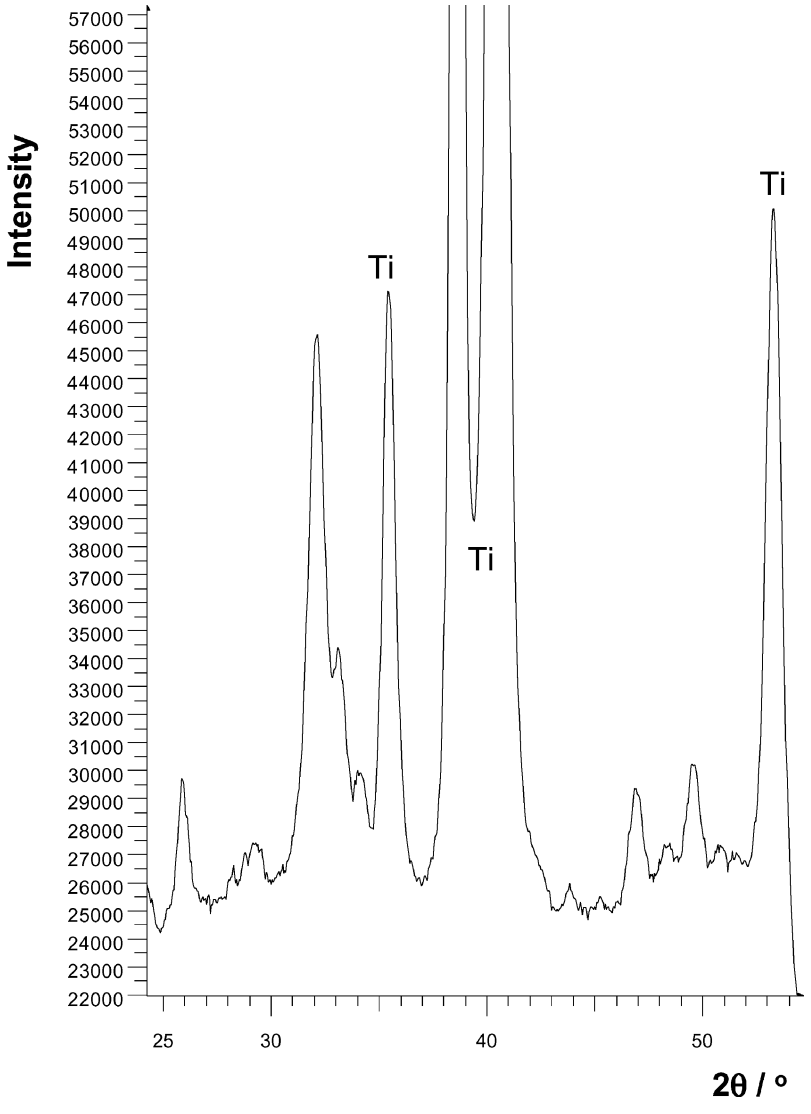

Figure 5 Diffractogram of ED material coating on a prosthetic stem. The principal Ti peaks are indicated and all the other peaks can be assigned to HAP. Note that the angular resolution and 2θ range are less than that of data measured by the conventional powder diffractometer.

demonstrated here although the relatively low degree of preferred orientation was consistent with previous studies.

Limitations of the methodology employed here for rapid quantitative composition determination include assuming constant absorption coefficients and no microabsorption. Further, the smooth function [33] used to model the increase in diffraction peak width with scattering angle, was deficient for the ED material. The basal reflections were not adequately modeled, as they had significantly smaller widths than predicted. This is a similar effect to that found in bone mineral and is due to the crystallites non-equiaxial morphology.

In order to confirm that material grown upon the test coupons within the ED bath could also be formed directly onto prosthetic substrates, we have also briefly examined coatings *in situ* on hip stems. These were examined by XRD using a Bruker D8 system with parallel optics and an X-ray area detector. The subsequent data were radially integrated and the resultant presented in Fig. 5. The Bragg maxima positions are a good match to HAP and the general form of the diffraction data very similar to that from the test coupon material. Therefore, we are confident that the material formed on the prosthetic surfaces is the same as that being examined on the test pieces.

Acknowledgements

We are indebted to Dr. Karen Hing (Queen Mary, UCL) for supplying the standard mixes of calcium phosphates. We are also grateful to Biomet-Merck for the supply of PS and ED coatings. Further, we wish to acknowledge the use of the EPSRC's Chemical Database Service at Daresbury.

References

1. J. D'ANTONIO, W. CAPELLO and W. JAFFE, *Clin. Ortho. Rel. Res.* **285** (1992) 102.
2. A. TONINO, L. ROMANINI, P. ROSSI, M. BORRONI, F. GRECO, C. GARCIA-ARAUJO, L. GARCIA-DIHINX, A. MURCIA, W. HEIN and J. ANDERSON, *Clin. Ortho. Rel. Res.* **312** (1995) 211.
3. C. YANG, B. WANG, E. CHANG and J. WU, *J. Mater. Sci: Mater Med.* **6** (1995) 249.
4. K. GIANNIKAS, R. DIN, S. SADIQ and T. DUNNINGHAM, *J. Arthro.* **17** (2002) 184.
5. N. COSTA and P. MAQUIS, *Med. Eng. Phys.* **20** (1998) 602.
6. M. SHIRKHANZADEH and G. LIU, *Mat. Let.* **21** (1994) 115.

7. J. M. ZHANG, *Chem. J. Ch. Univ.* **18** (1997) 961.
8. M. SHIRKHANZADEH, *J. Mater. Sci: Mat. Med.* **6** (1995) 90.
9. D. B. HADDOW, *ibid.* **10** (1999) 219.
10. SILVA DA, *Proc. Int. Symp. Ceram. Med.* **11** (1998) 233.
11. Y. HAN, *J. Mater. Sci: Mat. Med.* **10** (1999) 243.
12. M. SHIRKHANZADEH, *J. Mater. Sci. Lett.* **10** (1991) 1415.
13. J. M. ZHANG, C. J. LIN, D. Z. FENG and Z. W. TIAN, *J. Electroanalyt. Chem.* **452** (1998) 235.
14. S. OVERGAARD, U. BROMOSE, M. LIND, C. BUNGER and K. SOBALLE, *J. Bone Joint Surgery* **81** (1999) 725.
15. A. G. DELATORRE, S. BRUQUE and A. G. ARANDA, *J. Appl. Cryst.* **34** (2001) 196.
16. E. GIRARDIN, K. HIRSCHI and A. LODINI, *Mat. Man. Proc.* **13** (1998) 581.
17. L. KELLER and W. A. DOLLASE, *J. Biomed. Res.* **49** (2000) 244.
18. P. S. PREVEY, *J. Theraml Spray Tech.* **9** (2000) 369.
19. H. RIETVELD, *J. Appl. Cryst.* **2** (1969) 65.
20. P. RIELLO, N. CANTON, S. COMELATO, M. POLIZZI, G. VERITÀ, H. FAGHERAZZI, A. HOFMEISTER and S. HOPFE, *J. Non-Cryst. Solids* **288** (2001) 127.
21. K. LUDWIG, *J. Biomed. Mater Res.* **29** (1995) 1403.
22. D. A. FLETCHER, R. F. MCMEEKING and D. PARKIN, *J. Chem. Inf. Comput. Sci.* **36** (1996) 746.
23. L. KELLER and S. LYENGAR, presented to ASTM Committee F04.13.05 November 1993, Dallas.
24. W. TONG, Z. YANG, X. ZHANG, A. YANG, J. FENG, Y. CAO and J. CHEN, *J. Biomed. Mater Res.* **40** (1998) 407.
25. G. K. WILLIAMSON and W. H. HALL, *Acta Metal.* **1** (1953) 22.
26. C. M. ROOME and C. D. ADAM, *Biomaterials* **16** (1995) 691.
27. A. BROADHURST, K. ROGERS, D. LANE and T. LOWE, 52 nd Denver X-ray Conf. Aug. 2003, Denver.
28. L. YAN, Y. YANG LENG and L. WENG, *Biomat.* **24** (2003) 2585.
29. M. MANSO, C. JIMÉNEZ, C. MORANT, P. HERRERO and J. M. MARTÍNEZ-DUART, *ibid.* **21** (2000) 1755.
30. M. FULMER, I. ISON, C. HANKERMAYER, B. CONSTANTZ and J. ROSS, *ibid.* **23** (2002) 751.
31. M. SHIRKHANZADEH, *J. Mater. Sci.: Mat. Med.* **9** (1998) 67.
32. W. TONG, J. CHEN, X. LI, J. FENG, C. YANG, Y. YANG, J. ZONG and X. ZHANG, *J. Mater Sci.* **31** (1996) 3739.
33. G. CALGOTTI, A. PAOLETTI and F. RICCI, *Nucl. Inst. Meth.* **35** (1958) 223.

Received 30 July 2003
and accepted 11 November 2004